IOPscience iopscience.iop.org

Home Search Collections Journals About Contact us My IOPscience

Modelling of lattice and magnetic thermal disorder in manganese oxide

This article has been downloaded from IOPscience. Please scroll down to see the full text article.

1998 J. Phys.: Condens. Matter 10 9401

(http://iopscience.iop.org/0953-8984/10/42/006)

View the table of contents for this issue, or go to the journal homepage for more

Download details:
IP Address: 171.66.16.210
The article was downloaded on 14/05/2010 at 17:36

Please note that terms and conditions apply.

J. Phys.: Condens. Matter **10** (1998) 9401–9412. Printed in the UK PII: S0953-8984(98)95255-9

Modelling of lattice and magnetic thermal disorder in manganese oxide

A Mellergård†, R L McGreevy‡, A Wannberg‡ and B Trostell‡

† Materials Physics, KTH, S-100 44 Stockholm, Sweden

‡ Studsvik Neutron Research Laboratory, Uppsala University, S-611 82 Nyköping, Sweden

Received 18 June 1998

Abstract. The local atomic and magnetic structure of a powder crystalline sample of MnO has been modelled for a wide range of temperatures (10–1100 K) by fitting neutron powder diffraction data using the reverse Monte Carlo technique (RMC). This method allows simultaneous and self-consistent fitting of Bragg *and* diffuse scattering of both nuclear and magnetic origin and so the fitted models contain information not only on long-range order but also disorder. Results show that the method as applied to MnO produces models that give correct values for different known physical properties so that prospects for modelling less simple materials are good.

1. Introduction

Many crystalline materials have interesting properties, both scientifically and technologically, which are related to detailed magnetic and crystalline structures on a local scale. Recent advances in, for example, the so-called colossal magnetoresistance (CMR) perovskite materials, indicate an intimate coupling of conduction properties to the local lattice and spin structure [1]. However, most of the diffraction work on these and related materials concentrates on the long-range time-averaged crystal and magnetic structures corresponding to information in Bragg scattering. Only a few studies of the local order have been performed and these have not simultaneously considered the atomic *and* magnetic scattering present. The total scattering cross section, $F(Q) \equiv \mathrm{d}\sigma/\mathrm{d}\Omega$, measured in a powder diffraction experiment, includes both elastic (Bragg) scattering and energy-integrated inelastic (diffuse) scattering. As a consequence $F(Q)$, being essentially the Fourier transform of the radial distribution function, $g(\boldsymbol{r}) \equiv G(\boldsymbol{r}, t = 0)$ and its magnetic counterpart, the spin–spin correlation function $\langle\mu(0)\mu(\boldsymbol{r})\rangle$, provides information not only on average structure but also on the instantaneous picture of local distortions and fluctuations in the structure, which is clearly of crucial importance in understanding CMR and similar effects. So, if diffuse scattering is not considered then valuable information is lost. Results might even be misleading since the presence of diffuse scattering unavoidably influences the fitting of Bragg peaks [2]. In some cases integrated Bragg intensities could be overestimated by as much as 25% because of this effect.

A general method for including the effect of static and dynamic disorder is provided by the RMC technique [3]. The basic approach of this method is to fit the calculated total scattering cross section of a model, typically consisting of several thousands of atoms, to the experimental data, possibly from both neutron and x-ray diffraction, by a procedure

0953-8984/98/429401+12$19.50 © 1998 IOP Publishing Ltd

analogous to Monte Carlo simulation. The model scattering cross section is obtained as the Fourier transform of the radial distribution function computed for the model. Atoms are moved randomly and after each trial move the resulting calculated cross section is compared to experimental data. Moves are then accepted if the fit is improved, but to prevent trapping in local minima other moves are also allowed with a certain probability. Because the calculated cross section represents total scattering computed on an absolute scale suitable data must be measured, i.e. with proper normalization and background corrections so that no arbitrary or temperature dependent scaling parameters or offsets have to be invoked. This, of course, implies that data have to be of good quality, but also that there is a very strong consistency constraint on a fitted model. It must, at the same time, account for any long- or medium-range order as well as correlations on a short length scale as revealed by data. Originally designed for the study of liquids and amorphous materials, the method has been developed and applied to materials with less disorder, and also for modelling magnetic structure [3].

The present work was carried out as a test of a new RMC powder method, RMCPOW [4, 5], which can be used to model both the atomic and magnetic local structure in powder crystalline materials with the aim of studying for example polaron formation in CMR materials. Such relatively well ordered systems have strong coherent scattering features even at large Q and there are serious truncation errors when using the standard RMC procedure, involving the Fourier transform of the radial pair distribution function $g(r)$. In the RMC powder method (RMCPOW) this is replaced by a direct calculation of the total structure factor $F(Q)$ taking full advantage of periodic boundary conditions. Another issue in the analysis of diffraction data from CMR and similar materials is the treatment of magnetic scattering from 3d ions. Whether this is manifested by structureless paramagnetic scattering, well above the ordering temperature, or whether spins are correlated so that Bragg and/or diffuse magnetic peaks are observed, it cannot be completely neglected. Fitting the diffuse scattering on an absolute scale by inverse methods (i.e. modifying and Fourier transforming a real space model) without considering the magnetic part can lead to spurious features in the real space atomic structure. In the case of isotropic materials magnetic scattering can be included in the RMC method using the formalism of Blech and Averbach [6, 7]. For crystalline materials this is not applicable so in order to treat magnetic scattering from powder crystalline materials properly we also need to use a direct calculation of $F(Q)$.

It may be questioned as to why a method is being developed to model diffuse scattering from powders, whereas single crystal data could in principle provide much more information and with better signal-to-noise. In fact a similar method does exist for single crystal data [8] (though not including magnetic scattering), but there are still technical problems associated with its implementation and the results obtained so far (e.g. [9, 10]) have not been as successful as those for powders. Partly these problems are due to the fact that single crystal neutron diffraction instruments are not typically constructed appropriately for producing the type of data required by RMC methods (in particular the incident wavelength is usually too long, giving problems with inelastic scattering effects) and partly due to the difficulties of absolutely correcting and normalizing single crystal data. It should also be noted that often either suitable single crystals cannot be grown, or it is not possible to measure single crystal patterns at a large enough number of $\boldsymbol{Q}$ points and for a sufficient number of samples/temperatures within a realistic time scale. Powder data, therefore, have practical advantages.

MnO was chosen as a test system because of its well separated Bragg peaks and large magnetic moment giving rise to huge amounts of magnetic diffuse scattering around the Néel temperature, $T_N \approx 120$ K. Furthermore, the lattice and spin structure and dynamics have

been well studied both by experiment and calculations [11–14] so that we can compare the results of the new RMCPOW technique with those of other methods. Finally, from direct inspection of the predominantly magnetic scattering at low Q it is clear that spin correlations persist up to at least 1100 K. It has been suggested that this feature is related to some clustering of spins and that there might even be a phase transition from short-range order to paramagnetic behaviour (i.e. completely uncorrelated spins) at $\approx 3T_N$ [15, 16]. We believe that our results show that these spin correlations are not due to simple clustering of nearly collinear spins but can be described in terms of large-amplitude correlated spin oscillations.

2. Experiments

We have measured total structure factors, $F(Q)$, for MnO using neutron powder diffraction at the SLAD diffractometer at the Studsvik Neutron Research Laboratory [17]. The SLAD instrument is a medium-resolution diffractometer designed for the study of disordered materials. It is equipped with a large array of position-sensitive detectors offering the possibility of fast measurements with good signal-to-noise ratio over the entire scattering angle range corresponding to scattering vectors $Q = 0.4$ Å^{-1} to 10 Å^{-1}. For studies of diffuse magnetic scattering this property is obviously of particular importance at small Q. The sample was taken from a standard commercial batch of purity 99%. 5 g of powder was loaded into a thin-walled vanadium can with a diameter of 8 mm. Data have been obtained at 18 temperature points, ranging from 10–1100 K, using a commercial closed-cycle refrigerator and a custom-built furnace. Standard corrections for absorption, multiple scattering and inelasticity were applied using the CORRECT program [18]. Normalization was performed using data from a vanadium rod. The inelasticity corrections were calculated in the incoherent approximation, but since both phonon [12] and magnon [13] dispersions in MnO are limited to quite low energies (<50 meV) and the energy of the incident neutrons was 65 meV we expect this to be reasonably accurate.

Some examples of the experimental $F(Q)$ data are shown in figure 1. At 10 K the magnetic and nuclear scattering intensity is mostly concentrated in the Bragg peaks and the diffuse scattering is very weak. By magnifying the small Q part (as in figure 1(b)) we can see that the magnetic diffuse scattering is mainly confined to the neighbourhood of magnetic Bragg peaks. With increasing temperature the magnetic intensity moves progressively into the diffuse part and remains centred at Bragg positions. The spin disorder is thus clearly of a correlated nature as expected from spin wave theory. Above T_N magnetic Bragg peaks are absent but the diffuse part is still structured and approaches the limiting paramagnetic form only at the highest temperature investigated, 1100 K. The nuclear diffuse scattering shows a similar dependency with temperature to that which could be ascribed to the thermal excitation of phonons. Nuclear Bragg peaks are of course present at all temperatures, decreasing in intensity as nuclear diffuse scattering grows.

3. Calculations

The RMCPOW algorithm is based on calculation of the total neutron scattering cross section for a mesh of points in reciprocal space [5]. This is done by making the model a supercell of the crystal unit cell and applying periodic boundary conditions. Thus, model scattering is described by the allowed reciprocal vectors of the *supercell*. For a perfectly ordered model contributions to the scattering will be non-zero only for the subset of Bragg peaks

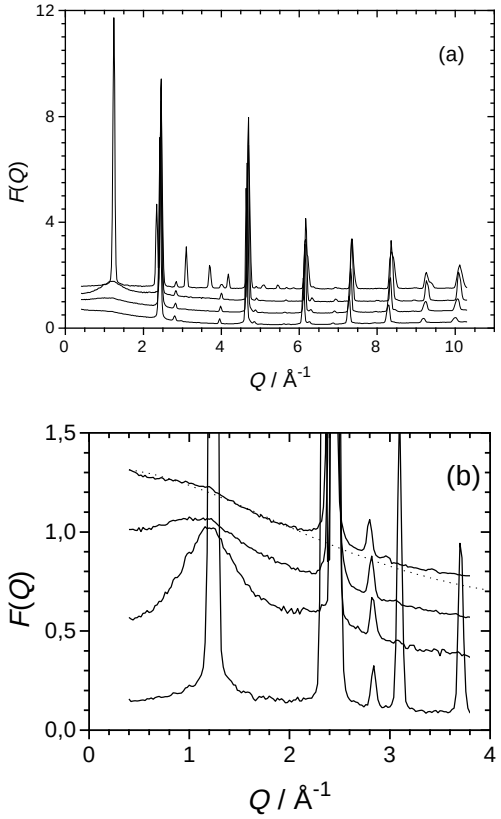

Figure 1. (a) Experimental $F(Q)$ (full curves) for MnO at (top to bottom) 10, 500, 900 and 1100 K; the successive offset is 0.5. (b) The small Q region shown on an expanded scale. Here the offset is 0.2 and the temperature sequence is reversed for visibility. The paramagnetic form factor, calculated with $S = 2.37$, is shown as a broken curve. As described in the text, this would be the limiting high-temperature shape of magnetic scattering.

of the *crystal* cell. If atoms are displaced from their equilibrium crystal sites then intensity will also appear in additional peaks, these effectively being the diffuse scattering of the disordered model crystal. It should be pointed out that models correspond to instantaneous pictures of the structure and therefore are not 'unique'. What is important is that they provide a physically consistent picture which is *in agreement with real data* in terms of the fit to experimental $F(Q)$, but also that other properties are obtained correctly as we will show later.

Formally, the diffuse part could be considered as originating from a Fourier expansion in terms of plane waves propagating with wavevectors in the first Brillouin zone of the *crystal* cell, of course limited in number by the multiplicity of crystal cells in the supercell, and so it is possible to describe coupled atomic displacements or spin oscillations with this construction, for example correlated harmonic vibrations. However, since we are moving atoms individually the fitted configurations can also correspond to a non-harmonic spectrum and contain multiphonon contributions or even isolated lattice distortions.

The crystal and ordered magnetic structures of MnO are shown in figure 2. The lattice structure is of rock-salt type with a small rhombohedral distortion below T_N. Below T_N

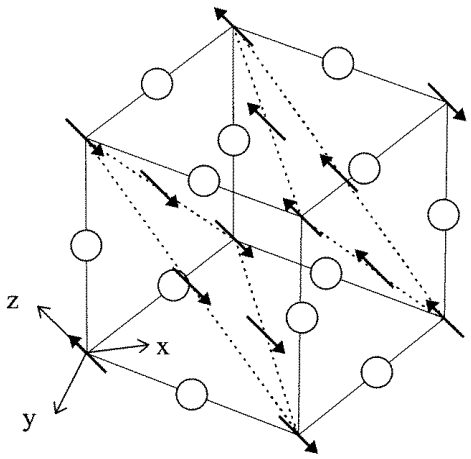

Figure 2. The cubic unit cell of MnO. Mn atoms are depicted by the orientation of their spin (↑) and oxygen by ○. Two pairs of anti-ferromagnetically coupled sheets are shown and the full magnetic cell is obtained by doubling along each lattice edge. The Cartesian coordinate system shown is that used for calculating the distribution of absolute spin orientations, as shown in figure 7.

the magnetic structure is built up of alternating spin-up and spin-down layers. These are perpendicular to the pseudo-cubic [111] direction with the magnetization easy-axis in one of the $\langle 1\bar{1}0\rangle$ directions within {111} planes [11]. For the purpose of setting up initial configurations, lattice parameters and Debye–Waller factors were obtained by Rietveld refinement of diffraction data. Starting lattice models were produced by applying Gaussian distributed random displacements, given by the refined thermal factors, to the average lattice positions at particular temperatures. In order to cope with the enlarged magnetic cell the corresponding hexagonal unit cell of MnO, having 48 atoms, was used at all temperatures. For simplicity this choice of crystal cell was also used in the RMCPOW calculations and the models were built from $(6 \times 6 \times 4)$ cells, containing 6912 atoms and 3456 spins. Linear dimensions are, therefore, about 35 Å within magnetic layers and 60 Å in perpendicular direction. For a given crystal symmetry one could, in principle, introduce lattice parameter refinement at each step in the RMCPOW algorithm. The change in terms of goodness-of-fit are expected to be small compared to using fixed (supercell) lattice parameters; the important difference compared to Rietveld refinement lies in computing the intensities, not positions, of Bragg and diffuse peaks. Modelling was, therefore, performed with constant supercell lattice parameters at each temperature. Data at all temperatures were modelled using 20 000–100 000 trial atom moves and 10 000–30 000 spin rotations, after which no significant improvement in fit was found. Given that the computing time for each move is about 1.5 s, calculations for all T were performed in less than one week of CPU time using a VAX4000 workstation.

4. Results

4.1. Lattice structure from nuclear scattering

For lower temperatures, $T < 300$ K, it was found that lattice diffuse scattering appeared to be well reproduced by random displacements in initial configurations. At higher temperatures

though, the average level systematically becomes too low, as might be expected because thermal factors were determined without correcting the Bragg intensity for thermal diffuse scattering. Also, the lack of correlated displacements in these initial models is reflected by the monotonous increase with Q of the calculated diffuse scattering. An example is given in figure 3; the broad diffuse features appearing under (nuclear) Bragg peaks are not present in the calculated cross section. This is probably also the case at lower temperatures, but here the diffuse peaks are so weak that they get lost under the Bragg peaks. After extensive RMC fitting the average level was reproduced correctly and the models could also reproduce diffuse peaks under Bragg peaks.

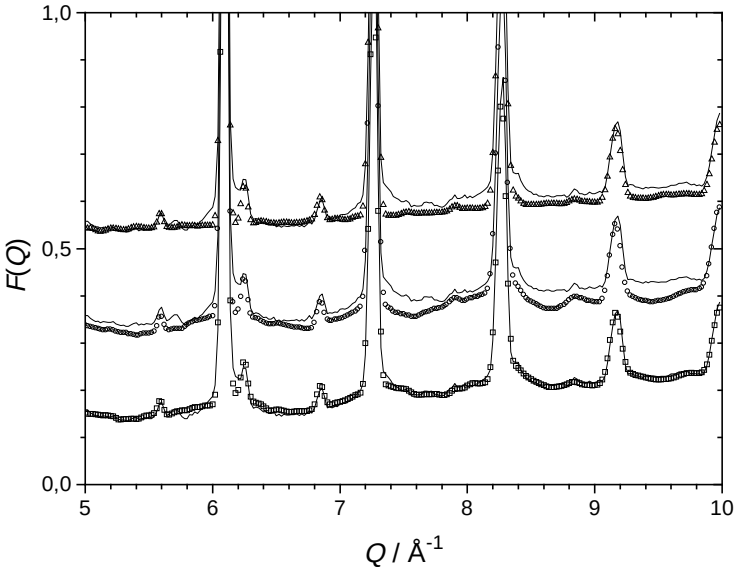

Figure 3. Experimental $F(Q)$ (full curves) together with those calculated from various models; random displacement configuration (△) based on Rietveld refined thermal factors, harmonic phonon displacements (○) and the RMCPOW fitted configuration (□). Each pair of curves is successively offset by 0.2.

As MnO is not expected to have any appreciable degree of static disorder diffuse scattering presumably arises mainly because of excitation of coupled vibrations, i.e. phonons. In order to verify this we have devised a simple model for dispersion of harmonic phonons in MnO and calculated the scattering cross section from a model with atomic displacements determined by such a spectrum. The exact solutions for longitudinal acoustic (−) and optic (+) phonons with wavevector k along the cubic [100] direction are

$$\bar{\omega}^2 = 2\left(\frac{2v_L}{a}\right)^2 \frac{(M_{Mn}+M_0)^2}{4M_{Mn}M_0}\left\{1 \pm \sqrt{1 - \frac{4M_{Mn}M_0}{(M_{Mn}+M_0)^2}\sin^2\left(\frac{ak}{2}\right)}\right\}.$$

Here, a is the cubic lattice constant and v_L is the longitudinal velocity of sound. Expressions for Mn and O atomic displacements are then given by these energies. The dispersion relations were generalized into three degenerate branches each for acoustic and optical phonons by replacing a in the expression above with π/k_D, where $k_D \approx 1.4$ Å^{-1} is the Debye wavevector cut-off. Phonon energies, and hence atomic displacements, were thus

determined only by the observed lattice parameters and the velocity of sound. Keeping the latter at 7200 m s^{-1} (deduced from an average over all directions of the phonon dispersion curves of [12]) we obtained models having diffuse peaks similar to those observed in the experimental data. Although the amplitude and shape of these peaks are approximately correct the average levels are even lower than those of random configurations (see figure 3). This is obviously due to anharmonic contributions becoming more important with increasing temperature.

We have calculated the mean square atomic displacements, $\langle \boldsymbol{u}^2 \rangle$, of the various models and the results are presented in figure 4. Here it can be seen that the general properties of crystals with NaCl structure are reproduced by RMCPOW fitted configurations. As T goes to zero $\langle \boldsymbol{u}^2(\mathrm{Mn}) \rangle$ and $\langle \boldsymbol{u}^2(\mathrm{O}) \rangle$ do not vanish; their ratio approaches the ratio of the atomic masses as expected for zero-point motion. At intermediate temperatures (300–600 K) there is a linear dependence on T; in this regime the particular property of NaCl structures, having equal $\langle \boldsymbol{u}^2 \rangle$ for both atom types, is confirmed. Finally, at the highest temperatures there is an extra non-linear contribution which is related to anharmonic vibrations. The latter property is clearly seen when we compare with $\langle \boldsymbol{u}^2 \rangle$ of the harmonic model, for which the same low- and intermediate-temperature behaviour is observed but at high temperature $\langle \boldsymbol{u}^2 \rangle$ maintains linear dependence of T. Note, that we do not propose this model phonon dispersion to be the correct one for MnO. It merely serves to give a picture of what diffuse scattering would look like in a reasonable phonon displaced configuration. The RMCPOW fitted models also show a larger non-linear contribution than the Rietveld results (or equivalently: initial random configurations), thus demonstrating that anharmonic effects are even larger than expected from Rietveld refinement.

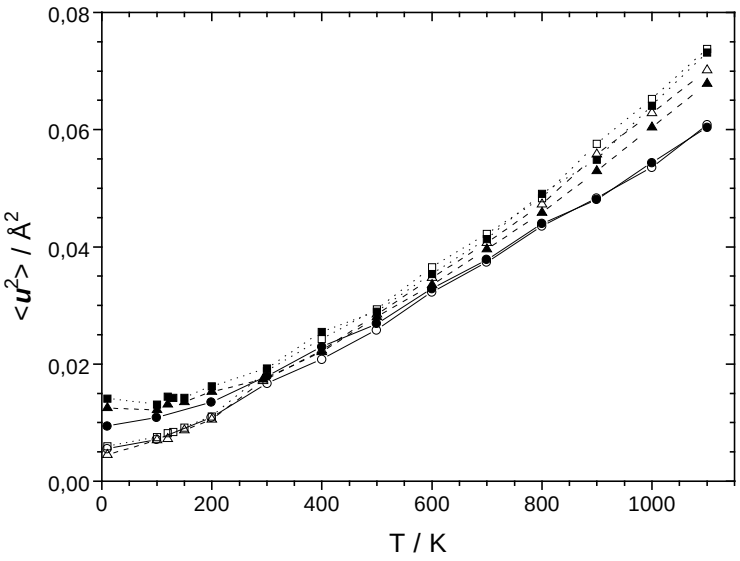

Figure 4. Mean square displacements of Mn (open symbols as in figure 3) and O (full symbols) atoms as a function of temperature for the various models shown in figure 3. The linear temperature dependence in the harmonic model, and therefore its shortcoming, is clearly seen. Non-linear contributions are seen to be even larger in the curves based on the RMCPOW fitted configurations than for the random configurations created using Rietveld refined thermal factors, showing that an enhanced degree of anharmonicity is obtained by also fitting diffuse scattering.

4.2. Magnetic structure

Since we are computing the magnetic cross section using classical spins the first step in setting up spin configurations was to find an appropriate value for the single-spin total magnetic moment $\mu = |\mu|$. For a free Mn^{2+} ion, with a Landé factor $g = 2$ and spin $S_{free} = 5/2$, we have $\mu_{free} = g\sqrt{S_{free}}(S_{free} + 1) = 5.92\ \mu_B$. Covalency effects on the magnetic moment of Mn^{2+} in MnO have been estimated to reduce the value of S_{free} by 3.6% so that $S_{cov} = 2.41$ and $\mu_{cov} = 5.73\ \mu_B$ [14]. Considering the amplitude of the limiting paramagnetic form-factor at high temperature we found that at 1100 K best agreement of the small-Q data with a paramagnetic structure factor was obtained for a spin $S = 2.37$, in fair agreement with the covalency reduction. Using this value, i.e. $\mu = 5.65\ \mu_B$, we obtained the correct amount of both Bragg and diffuse magnetic scattering throughout the whole temperature range in the RMCPOW calculations, thus demonstrating that we do indeed have good experimental data and a self-consistent modelling method.

According to spin wave theory [19] one can construct the ground state of a Heisenberg antiferromagnet starting from the Néel state where all spins are aligned to some axis, say z, having a maximum projection $|S_z| = |\pm S|$. In addition, zero-temperature correlated spin fluctuations will be present which further reduce $\langle S_z \rangle$. For MnO this reduction has been calculated to be of the order of 2.8% [14]. From Rietveld refinement of our data at 10 K we obtained $\langle S_z \rangle = 2.28$ for the average value of the projected spin, which indicates a zero-point spin reduction of 3.8% when compared to $S = 2.37$, in reasonable agreement with the calculation.

As a first attempt to create an initial spin model for the 10 K data we started from a maximum projection configuration, i.e. $S_z = +S$ for all spins on the spin-up sublattice and $S_z = -S$ on the spin-down sublattice, where the z-axis is in the average spin direction as given by Rietveld refinement. The azimuth angles (in the so defined xy-plane) were chosen randomly. From figure 5 it can be deduced that this construction gives too much paramagnetic character to the calculated diffuse scattering, in particular below $Q = 1$ Å^{-1}, even compared to the data at 10 K. If some additional zero-point spin oscillations were introduced in this configuration we do not expect this paramagnetic part to decrease, rather some structured magnetic diffuse scattering would appear on top of this level and be centred on the magnetic Bragg peaks, reducing the intensity of the latter. We believe that this indicates that the deviations from *full* projection of spins (on the average z-axis) take place

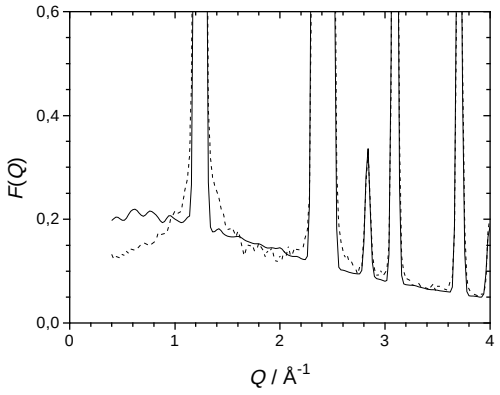

Figure 5. Detail of the experimental (full curve) and calculated (broken curve) $F(Q)$ at 10 K for a 'maximum-projection' model, as explained in the text.

in a correlated way, although it might be an artefact because of the classical treatment of spin orientations.

For the actual RMCPOW fit at 10 K we therefore started from the fully aligned state, i.e. $S_x = S_y = 0$ and $S_z = \pm\sqrt{S}(S+1)$. By calculating the statistics of the spin orientations in the fitted configuration, we found that $\langle S_z \rangle = 2.26$ so that this method also gives a good limiting value for zero-point deviations, again only constrained by the fit to data. This is, of course, related to the fit of the Bragg peaks but it is important to note also that the diffuse model scattering comes out with correct level and shape (see figure 6). Looking in more detail at the orientation of spins on one sublattice, relative to the average magnetization axis, we see that the distribution (shown in figure 7) does not peak at $S_z = S$, ($\cos\theta = 0.8$), as expected from quantum mechanics. Instead a large fraction of the spins still have almost full z-axis projection but are balanced by equal amounts of spins having large off-z-axis orientations, giving the expected $\langle S_z \rangle$ value. Clearly this comes about because of using classical spins, but we believe that there is nevertheless important information on the correlation of spin orientations. If we consider the projection of the spins onto the plane perpendicular to this axis we find that the distribution as a function of the azimuth angle in the plane, ϕ, is almost uniform so that there is no anisotropy about the average spin axis. This property would, of course, also be observed in a spin configuration with random azimuth angles, but as seen in figure 5 this would not give diffuse peaks.

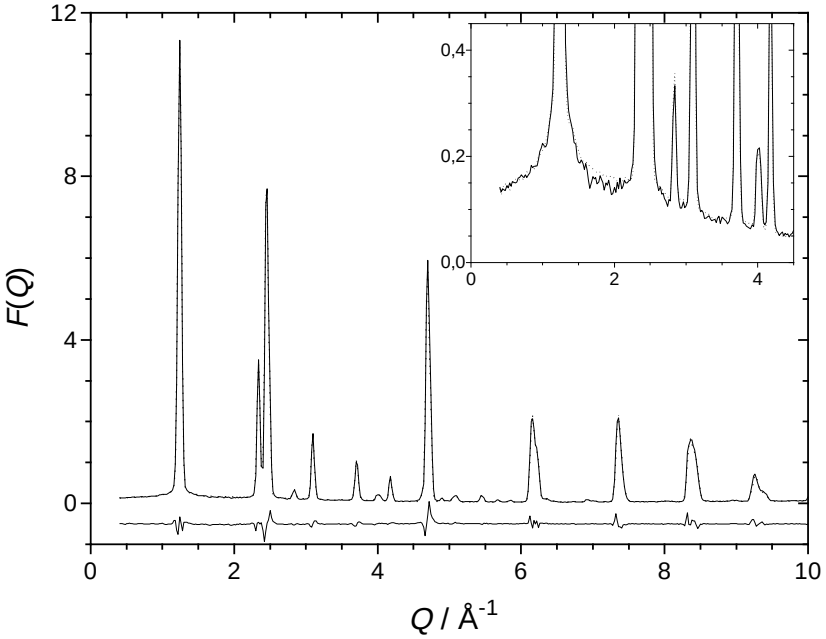

Figure 6. Experimental (full curve) and RMCPOW fitted $F(Q)$ (broken curve) at 10 K, together with the difference (lower curve). The inset shows the diffuse part at small Q on an expanded scale.

At higher temperatures the fitted magnetic diffuse scattering continues to agree well with the experimental data although it appears to be somewhat oscillatory since the most intense magnetic scattering is now seen at low-Q where the linear density of reciprocal vectors is small. Fitted spin configurations were successively used as starting points for the

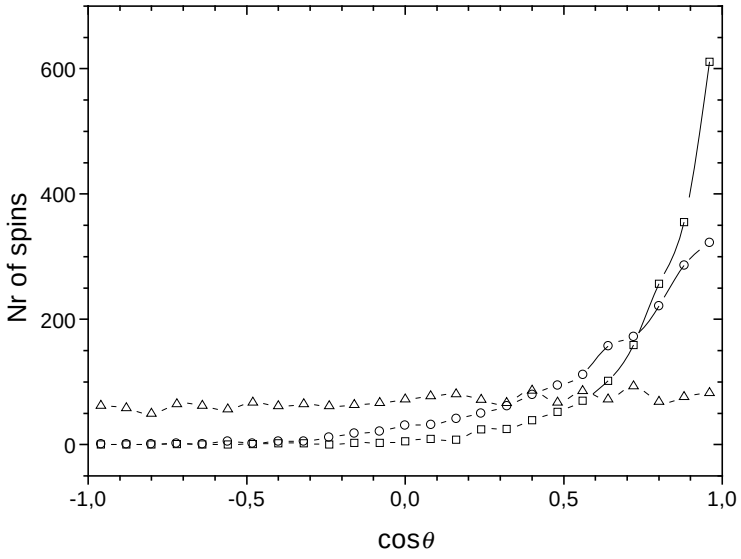

Figure 7. The distribution of spin orientations relative to the original spin-up axis at 10 K (□), 100 K (○) and 1100 K (△). Intermediate temperature distributions (120–1000 K) appear almost as featureless as that at 1100 K (see figure 8 and the text).

next higher temperature. In figure 7 it can be seen that the spin orientations, relative to the original magnetization axis, are rapidly approaching a uniform distribution above T_N. Now, each spin has six nearest neighbours on the same sublattice at a distance of ∼3.1 Å, ferromagnetically aligned at $T = 0$ K, and six on the other sublattice, anti-ferromagnetically aligned. Next nearest neighbours are all on the other, anti-parallel, sublattice separated by ∼4.4 Å. To quantify the deviations from this arrangement at non-zero temperatures we have calculated the average cosine of the spin–spin relative orientations, $\langle \cos\theta_r \rangle$, for the neighbour distances mentioned earlier, resolved into spin pairs that are originally parallel or anti-parallel (as defined at $T = 0$). As can be seen in figure 8, $\langle \cos\theta_r \rangle$ shows the expected decrease at T_N, indicating the loss of long-range order. More importantly we find that the $\langle \cos\theta_r \rangle$ values do not vanish above T_N but remain non-zero all the way up to 1100 K. The originally parallel nearest neighbour spins even show an average anti-parallel arrangement just above T_N. A possible explanation for this behaviour could be related to the fact that the exchange interaction parameters J_1^p and J_1^a for parallel and anti-parallel nearest neighbours, respectively, are both negative and almost equal [14] since both types of neighbours are roughly at the same distance. At low temperature the frustration created by this situation is relaxed by rhombohedral distortion so that $J_1^p < J_1^a$ and the spins can be almost fully ordered. By increasing temperature above the transition point makes it possible to have a small net anti-parallel arrangement of all nearest neighbours without any lattice distortion. Next nearest neighbours are all on the other sublattice so that such pairs, with J_2 also negative, apparently can have a relatively larger anti-parallel correlation at each temperature.

Another interesting property of the fitted spin configurations is that Bragg and diffuse magnetic scattering appear to depend on atomic displacements only through their mean square values at all temperatures. If the cross section calculation is repeated with the fitted spin configuration and new atomic configuration with random displacements based on mean square displacements in the fitted atomic configuration, then the new magnetic diffuse cross

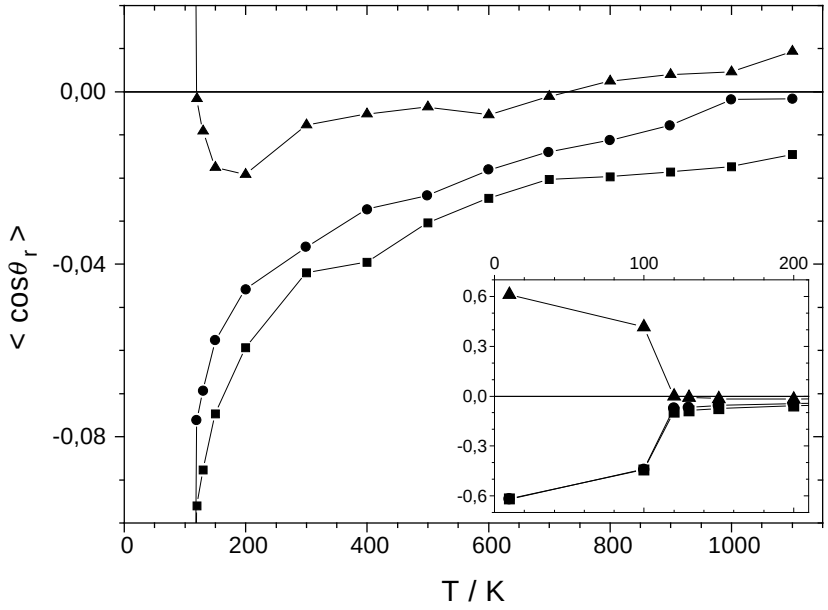

Figure 8. Average relative orientation of spins for some of the first neighbour distances; parallel (as defined at zero temperature) (▲) and antiparallel (●) neighbours at 3.1 Å and antiparallel neighbours (■) at 4.4 Å.

section is virtually identical to the previous one without further fitting. Consequently, there is no strong coupling of lattice and spin fluctuations in the fitted configurations, as anticipated for this fairly localized system. Finally, as also expected, the calculated magnetic Bragg intensities were found to decrease with the same Debye–Waller factor as for Mn nuclear scattering.

5. Conclusions

We have demonstrated that the RMC powder technique can reproduce experimental diffraction data for MnO over a wide temperature region and that the resulting configurations are consistent with known properties such as Debye–Waller (D–W) factors, zero-temperature atom and spin deviations etc. Given this good agreement with known properties we believe that the models must also contain realistic information on properties less well known, for example, information on the spatial arrangement of thermally disordered spins actually looks like in a real material, going beyond linear spin wave theory. The prospects for modelling more complicated structures should also be good.

In the present case of MnO we find that our results do not support the cluster picture where spins remain locally almost completely aligned above T_N. Nor can we find any evidence for a short-range phase transition; local correlations seem to disappear smoothly as a function of temperature. We also claim that spin deviations in MnO from full projection onto the average spin axis take place as zero-point correlated spin fluctuations. Below T_N one can certainly ascribe the observed magnetic diffuse scattering to the presence of magnons and we also believe that the high-temperature results are mostly due to large-amplitude correlated spin waves.

Acknowledgments

Support by the Swedish Natural Sciences Research Council and the Knut and Alice Wallenberg foundation is gratefully acknowledged.

References

[1] Ramirez A P 1997 *J. Phys.: Condens. Matter* **9** 8171
[2] Willis B T M and Pryor A W 1975 *Thermal Vibrations in Crystallography* (Cambridge: Cambridge University Press) pp 232–44 and references therein
[3] McGreevy R L 1995 *Nucl. Instrum. Methods* A **354** 1
[4] Montfrooij W, McGreevy R L, Hadfield R A and Andersen N-H 1996 *J. Appl. Cryst.* **29** 285
[5] Mellergård A and McGreevy R L *Acta Crystallogr.* A submitted
[6] Blech I A and Averbach B L 1964 *Physics* **1** 31
[7] Keen D A and McGreevy R L 1991 *J. Phys.: Condens. Matter* **3** 7383
[8] Nield V M, Keen D A and McGreevy R L 1995 *Acta Crystallogr.* A **51** 763
[9] Nield V M and Whitworth R W 1995 *J. Phys.: Condens. Matter* **7** 259
[10] Proffen Th and Welberry T R 1998 *J. Appl. Cryst.* **31** 318
[11] Roth W L 1958 *Phys. Rev.* **111** 772
[12] Haywood B C G and Collins M F 1968 *J. Phys. C: Solid State Phys.* **2** 46
[13] Pepy G 1974 *J. Phys. Chem. Solids* **35** 433
[14] Jacobson A J, Tofield B C and Fender B E F 1973 *J. Phys. C: Solid State Phys.* **6** 1615
[15] Hermsmeier B, Osterwalder J, Friedman D J and Fadley C S 1989 *Phys. Rev. Lett.* **62** 478
[16] Dräger K and Kratz G 1976 *Z. Naturforsch.* **31a** 1630
[17] Wannberg A, Delaplane R G and McGreevy R L 1997 *Physica* B **234** 1155
[18] see ftp://www.studsvik.uu.se/Pub/correct/
[19] For a comprehensive review Lovesey S W 1984 *Theory of Neutron Scattering from Condensed Matter* vol 2 (Oxford: Oxford University Press) pp 56–146